DOI 10.31489/2022No3/23-28

UDC 538.97

ELECTRON KINETICS OF YTTRIUM IRON GARNET AFTER SWIFT HEAVY ION IMPACT

Rymzhanov R.A.[1,2,*], Volkov A.E.[2,3], Ibrayeva A.D.[1,4]

[1]The Institute of Nuclear Physics, Almaty, Kazakhstan; r.a.rymzhanov@gmail.com
[2]Joint Institute for Nuclear Research, Dubna, Moscow Region, Russia;
[3]Lebedev Physical Institute of the Russian Academy of Sciences, Moscow, Russia;
[4]Centre for HRTEM, Nelson Mandela University, Port Elizabeth, South Africa;

The TREKIS Monte-Carlo model was applied to study the temporal electronic kinetics of yttrium iron garnet after a swift heavy ion impact. Cross sections of incident particles interaction with the target were determined within complex dielectric function-dynamic structure factor formalism. We found two modes of the spatial propagation of electronic excitation: fast delta-electrons form a front of the excitation while electrons produced due to decay of plasmons generated in a track form the second front slowly following behind the first one. Analysis of mechanisms of target lattice heating pointed to an important contribution of the potential energy released due to recombination of valence holes generated in an ion track. An increase of the excess lattice energy due to elastic scatterings of electrons and holes described with Mott cross-sections is minor. In contrast, complex dielectric function formalism demonstrates the significant contribution of these processes to the heating of the lattice.

Keywords: swift heavy ion track, electron excitations, complex dielectric function, ion energy loss, Monte Carlo simulations.

Introduction

Irradiation with swift heavy ions (SHI) decelerated due to the ionization processes can be applied as an effective tool for modification of solids, considerably changing material properties on the nanometric scale. The largest part of an energy deposited by an SHI is spent on excitation of the electron subsystem of a material [1,2]. Parameters of the initially excited electron ensemble determines subsequent kinetics of the electronic and atomic subsystems in the nanometric vicinity around the SHI trajectory [3]. The modification of the physical, chemical and mechanical properties of a target by SHI irradiation on nanometric level allows to use it in various nanostructuring applications [4–7].

Knowledge of cross-sections of charged particle scatterings on coupled target electrons as well as lattice atoms allows tracing the kinetics of material excitation along the ion trajectory that forms a basis for description of nonequilibrium structure modifications in SHI tracks. In this paper the complex dielectric function (CDF) formalism [8–10] is implemented to determine these cross sections for yttrium iron garnet ($Y_3Fe_5O_{12}$, YIG). The formalism takes automatically into account collective modes of electronic excitations in the target. Calculated cross sections of an SHI, electrons and valence holes scattering are then incorporated into the Monte-Carlo (MC) model describing coupled electronic and lattice kinetics in SHI tracks. Further, we analyze and compare contributions of different processes of electron-to-atoms energy transfer to lattice heating of YIG and Al_2O_3 in ion tracks.

1. Model

Based on asymptotic trajectories algorithm, the event-by-event simulations [11,12] of charged particles propagation forms the main principle of the MC code TREKIS [13,14]. We use the dynamic structure factor (DSF) formalism for determination of probabilities of charged particles interaction with a solid [8]. The dynamic structure factor can be declared as a product of the energy loss function (ELF), or the inverse imaginary part of the complex dielectric function (CDF) of a material. We reconstruct the ELF from the experimental and theoretical optical data as a set of artificial Drude oscillators [9,15], which gives us an

.

ability to describe partial cross-sections of electron interaction with the valence band and core shells as well as with the target lattice.

The TREKIS models: (a) propagation of an SHI producing ionization of a target and generation of free electrons (δ-electrons), holes in the valence band (VB) and deep atomic shells; (b) free δ-electrons interactions with ionic and electronic subsystems as well as subsequent kinetics of secondary electronic cascades forming due to relaxation of the excitation; (c) Auger decays of core holes, also forming secondary electrons; (d) radiative decays of deep shell holes, subsequent photon transport and photoabsorption, which produces new holes and electrons; (e) valence holes transport and their energy transfer to the lattice [13,14]. All details of the model assumptions and numerics of the code were thoroughly described in [13,14].

We analyze two channels of lattice excitation in the present approach: (1) due to elastic scattering of electrons and valence holes on the atomic system and (2) heating after release of the potential energy of the excited electron ensemble into the lattice due to recombination of valence holes. To describe this release, we assume an instant transfer of the excess potential energy of valence holes to the target atoms at 100 fs after the ion impact. Our previous works, Ref. [16,17], illustrated reliability of the applied approximation.

The MC procedure is iterated for ~103 times to obtain a trustworthy statistic for spatial and temporal distributions of parameters characterizing the excitation of a target: densities and energy densities of electrons, atoms, valence band holes and core holes in the proximity of an SHI track. These distributions can serve as input parameters (initial conditions and/or source terms) in further MD modeling of the kinetics of a lattice relaxation, structural modifications and phase transitions caused by an SHI passage [18,19].

2. Results and discussion

2.1. Construction of energy loss function

The energy loss function of YIG was reconstructed using ab-initio calculated optical properties from [20] and x-ray attenuation length from [21]. Figure 1a presents the loss function curve consisting of the set of peaks arising from peculiarities of photon interaction with the valence band and deep shells. We found in the literature data only for limited energy range for optical coefficients originated from the VB, so the intermediate energy region in Fig.1 was approximated to fulfill the sum rules. The scattering of excited electrons on atomic ensemble is described using Mott atomic cross sections with modified Molier's screening parameter [22,23] since no optical data describing phonon modes of YIG exist in the literature.

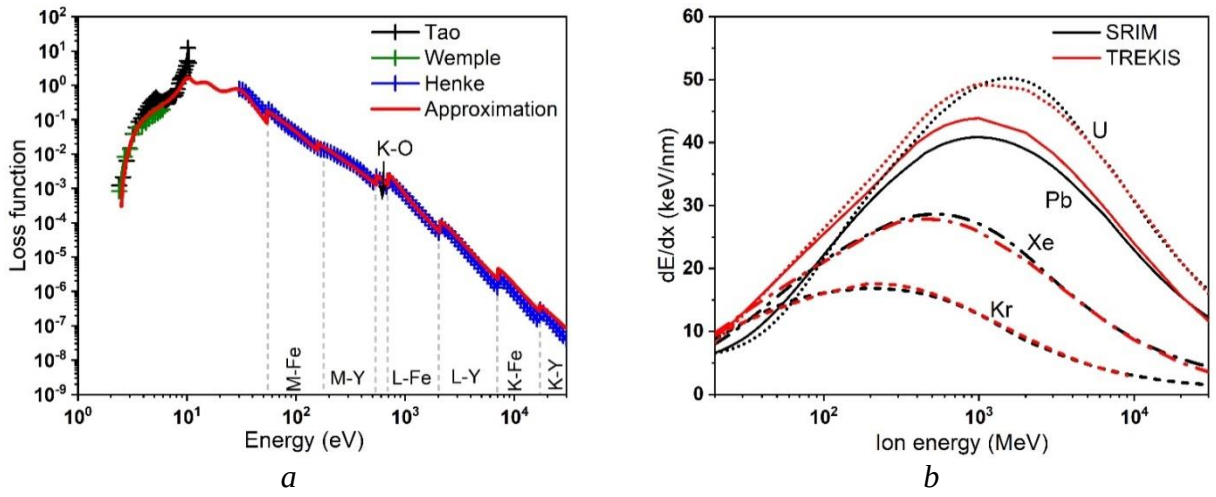

Fig.1. (a) Energy loss function of YIG obtained using experimental and theoretical optical data from: Tao [20], Henke [21] and Wemple [27]. (b) Energy dependent energy losses of different ions in YIG compared with SRIM code [25].

Table 1 collects the coefficients of the energy loss function of yttrium iron garnet in form of optical oscillators [9,13,26]. In this Table f-sum rule corresponds to the number of electrons (N_e) on a specific atomic shell and coincides very well with values from [27] (in brackets). The accuracy of the obtained ELF coefficients was verified by comparison of the calculated energy losses of different ions in YIG (Fig. 1b) with the SRIM code [25]. An overall good agreement confirms an applicability of the obtained fitting coefficients for the determination of cross sections of charged particles interaction with a solid YIG.

Table 1. Coefficients of the complex dielectric function of YIG in the form of oscillator functions. E_0, A, γ are coefficients of Drude-like oscillators [9, 13,26] used for ELF approximation. *f*-sum is the number of electrons (N_e) on the atomic shells. The values from [27] are shown in brackets for comparison.

Shell	E_0	A	γ	*f*-sum (N_e)
Valence band	3.1	-0.74	2.7	90.999 (91)
	10.2	30	2.5	
	15	114	8	
	30	380	18	
M-Fe	54	504	90	70.06 (70)
M-Y	157	532	400	78.01 (78)
K-O	540	202	340	23.997 (24)
L-Fe	700	338	350	39.999 (40)
L-Y	2100	192	1600	24.06 (24)
K-Fe	7000	83	5000	9.98 (10)
K-Y	17000	46	20000	5.98 (6)
Total:				343.09 (343)

2.2. Kinetics of the electron ensemble

Figure 2a presents temporal evolution of the radial energy density distributions of electrons in YIG calculated with MC TREKIS. We used Bi ions with 700 MeV energy, providing the energy losses of 43.6 keV/nm in YIG. Figure 2a demonstrates propagations of two fronts outwards from the ion trajectory. Movement of fast primary δ-electrons produced directly by the ion forms the first front.

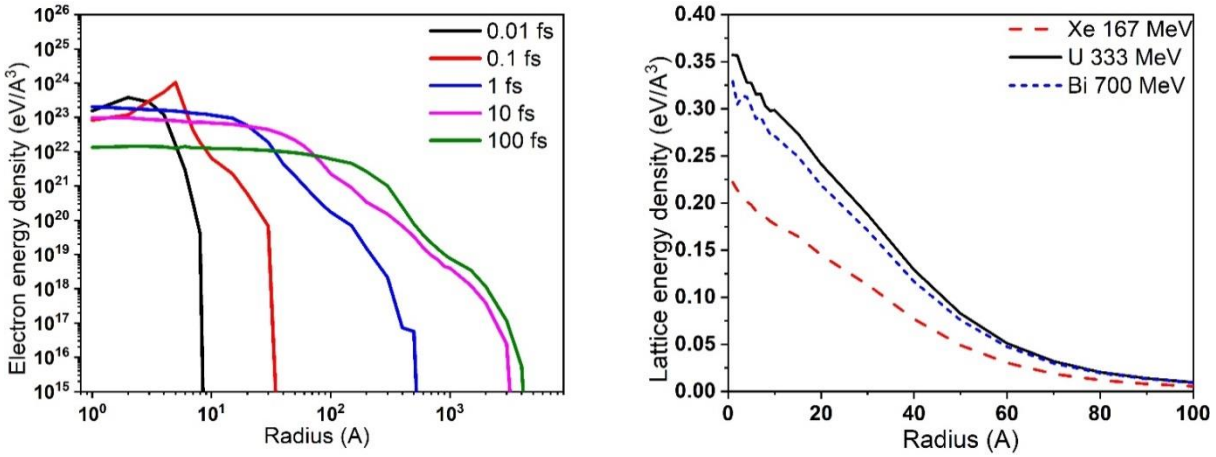

a b

Fig.2. (a) The radial electron energy distributions around the trajectory of 700 MeV Bi ion in YIG at different times; (b) radial lattice energy distribution in tracks of different ions at 100 fs.

The second one results from generation of a large number of secondary electrons with the energies around the plasmon peak in the valence band. We assume that these electrons with approximately the same energy are generated due to fast decay of plasmons appeared in the ion track. Subsequent collective propagation of these electrons outwards from the center of excited area forms the front in the spatial energy density at earlier times (< 1 fs) which then smoothens out by the time of 10 to 100 fs.

Electrons spreading out of the track core interact inelastically with target atoms (producing new electrons and holes) and elastically (transferring a part of their energy to the atomic subsystem). Figure 2b shows the distribution of excess lattice energy, which consists of three main contributions: elastic scattering

.

of electrons, energy transfer by spreading valence holes and the potential energy release due to recombination of valence holes. As was discussed in [28] this potential energy may be quickly (at 100 fs timescale) converted into the kinetic energy of atoms due to changes of the interatomic potential stimulated by the highly excited electron system. We approximate this energy increase by the band gap energy (per one valence hole remaining in a track by the time of 100 fs after ion passage). This energy is assumed to be instantly transferred to atoms at 100 fs [16].

Figure 3 compares dependencies of the energy transferred into YIG and Al_2O_3 lattices on the kinetic energy of scattered electrons and valence holes in a track of 167 MeV Xe ion. For comparison, we show the results of applications of two forms of elastic cross-sections in alumina: the Mott atomic approximation and scattering on optical phonons using CDF-DSF formalism.

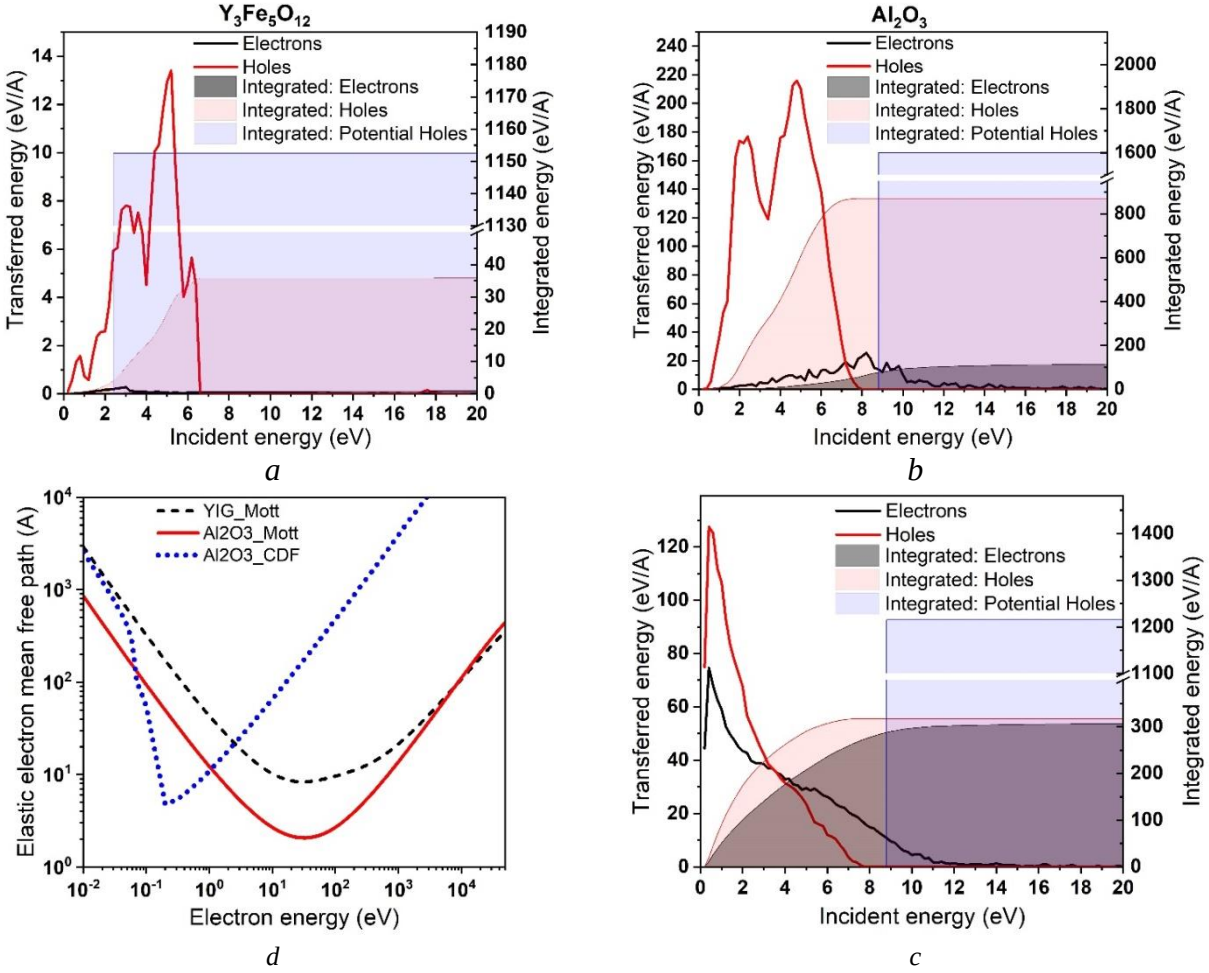

Fig.3. Dependence of the total energy transferred to the lattice by electrons and valence holes in 167 MeV Xe track on the particle kinetic energy in (a) YIG and (b) Al_2O_3 calculated using Mott atomic cross-sections, (c) Al_2O_3 calculated within CDF phonon cross-sections. Filled area shows the integrated elastic energy transfer by electrons/holes (grey and red) and potential energy of valence holes (blue). (d) Electron elastic mean free paths in YIG and Al_2O_3.

The potential energy distribution of valence holes is not shown in this Figure but it can be represented as a delta-function located at the band gap energy (2.4 eV for YIG and 8.8 eV for Al_2O_3). Blue filled rectangles represent the total excess energy accumulated by the lattice due to release of the potential energy of valence holes, which may constitute up to 65% of total lattice energy in alumina and about 97% in YIG.

Figure 3a also demonstrates that the almost all rest lattice energy (~3 %) for YIG is delivered by elastic interaction of valence band holes with target atoms, whereas electron scattering contributes less than 0.1 % of the total energy, when the Mott cross-section describes the both scattering processes. Almost all lattice energy is transferred by holes with energies below 6 eV.

In contrast to YIG, contributions of elastic scatterings of electrons and holes into heating of Al_2O_3 lattice is much larger: 4% for electrons and 32% for valence holes when the Mott cross section are used

(Figure 3b). Application of the phonon cross-sections gives the almost equal fractions of elastic channels of the energy transfer to the alumina lattice: ~17% for electrons and the same for valence holes (Figure 3c).

The registered difference between YIG and Al_2O_3 can be attributed to difference of atomic mass: the lower atomic masses in Al_2O_3 result in the higher probability of electron scattering (Figure 3d) on the lattice and the larger energy transfer to an atom in one impact.

It can be found, that the largest part of the energy transferred to lattice is provided by electrons and holes of energies below 10 eV. The maximum of the described by Mott cross-sections energy transferred by electrons is located at energies of ~8 eV (Figure 3b) whereas CDF cross sections result in maximum located at the much lower energies (< 0.5 eV). This difference reflects the positions of minima of the electron mean free path (inverse cross section) to elastic scattering on lattice (Figure 3d).

Conclusions

We present the results of simulations of electron subsystem excitation in swift heavy ion tracks in YIG performed with the help of the TREKIS MC code. The complex dielectric function formalism was applied to develop scattering cross sections and the energy losses of charged particles in YIG. Applicability of this approach was confirmed by a good agreement of calculated data with results of application of SRIM code [24].

Time resolved calculations revealed propagation of two fronts of electronic excitation. Fast δ-electrons form the first front while the second one behind it is attributed to electrons appearing due to decays (within 10 to 100 fs) of plasmons produced by excitation of electron ensemble.

Contributions of elastic scattering of electrons and valence holes to heating of the atomic subsystem were investigated. We show that the majority (~97%) of the lattice energy for YIG is delivered by conversion of the potential energy of valence holes, whereas contribution of elastic scatterings of electrons and holes is minor. In contrast to YIG, Al_2O_3 demonstrates the comparable contributions of these processes to the heating of the lattice. Electrons and holes of energies below 10 eV provide largest part of lattice energy transferred to the lattice via the elastic scattering channel in both materials.

Acknowledgments

Financial support from the Ministry of Education and Science of the Republic of Kazakhstan [grant number AP09259476] is acknowledged.

This work has been carried out using computing resources of the Federal collective usage center Complex for Simulation and Data Processing for Mega-science Facilities at NRC “Kurchatov Institute”, http://ckp.nrcki.ru/, as well as computing resources of GSI Helmholtz zentrum (Darmstadt, Germany) and the Hybri LIT heterogeneous computing platform (LIT, JINR, http://hlit.jinr.ru).

REFERENCES

1 Komarov F.F. Defect and track formation in solids irradiated by superhigh-energy ions. *Physics-Uspekhi*. 2003. Vol. 46, pp. 1253–1282.

2 Miterev A.M. Theoretical aspects of the formation and evolution of charged particle tracks. *Physics-Uspekhi*. 2002. Vol. 45, pp. 1019–1050.

3 Baranov A.A., Medvedev N.A., Volkov A.E., et al. Effect of interaction of atomic electrons on ionization of an insulator in swift heavy ion tracks. *Nuclear Instruments and Methods in Physics Research B.* 2012. Vol. 286, pp. 51–55.

4 Komarov F.F. Nano- and microstructuring of solids by swift heavy ions. *Physics-Uspekhi*. 2017. Vol. 60, pp. 435–471.

5 Wesch W., Wendler E. *Ion Beam Modification of Solids, Ion-Solid Interaction and Radiation Damage*. Berlin: Springer, Cham, 2016, 534 p.

6 Jana K.K., Ray B., Avasthi D.K., Maiti P. Conducting nano-channels in an induced piezoelectric polymeric matrix using swift heavy ions and subsequent functionalization. *Journal of Materials Chemistry*. 2012. Vol. 22, pp. 3955.

7 Kozlovskiy A.L. Study of the wear resistance degradation kinetics of aln ceramic under heavy ion irradiation. *Eurasian Physical Technical Journal.* 2022. Vol. 19, pp. 10–14.

8 Van Hove L. Correlations in Space and Time and Born Approximation Scattering in Systems of Interacting Particles. *Physical Review*. 1954. Vol. 95, pp. 249–262.

9 Ritchie R.H., Howie A. Electron excitation and the optical potential in electron microscopy. *Philosophical*

.

Magazine. 1977. Vol. 36, pp. 463–481.

10 Boutboul T., Akkerman A., Breskin A., Chechik R. Electron inelastic mean free path and stopping power modelling in alkali halides in the 50 eV–10 keV energy range. *Journal of Applied Physics*. 1996. Vol. 79, pp. 6714.

11 Eckstein W. *Computer Simulation of Ion-Solid Interactions*. Berlin, Heidelberg: Springer Berlin Heidelberg, 1991, 296 p.

12 Gervais B., Bouffard S. Simulation of the primary stage of the interaction of swift heavy ions with condensed matter. *Nuclear Instruments and Methods in Physics Research B.* 1994. Vol. 88, pp. 355–364.

13 Medvedev N.A., Rymzhanov R.A., Volkov A.E. Time-resolved electron kinetics in swift heavy ion irradiated solids. *Journal of Physics D: Applied Physics*. 2015. Vol. 48, pp. 355303.

14 Rymzhanov R.A., Medvedev N.A., Volkov A.E. Effects of model approximations for electron, hole, and photon transport in swift heavy ion tracks. *Nuclear Instruments and Methods in Physics Research B*. 2016. Vol. 388, pp. 41–52.

15 Rymzhanov R.A., Medvedev N.A., Volkov A.E. Monte-Carlo modeling of excitation of the electron subsystem of Al2O3 and polyethylene after swift heavy ion impact. *Nuclear Inst. and Methods in Physics Research B.* 2014. Vol. 326, pp. 238–242.

16 Rymzhanov R., Medvedev N.A., Volkov A.E. Damage threshold and structure of swift heavy ion tracks in Al2O3. *Journal of Physics D: Applied Physics*. 2017. Vol. 50, pp. 475301.

17 Terekhin P.N., Rymzhanov R.A., Gorbunov S.A., et al. Effect of valence holes on swift heavy ion track formation in Al2O3. *Nuclear Instruments and Methods in Physics Research B*. 2015. Vol. 354, pp. 200–204.

18 Ridgway M.C., Bierschenk T., Giulian R., et al. Tracks and Voids in Amorphous Ge Induced by Swift Heavy-Ion Irradiation. *Physical Review Letters*. 2013. Vol. 110, pp. 245502.

19 Rymzhanov R.A., Medvedev N., Volkov A.E., O'Connell J.H., Skuratov V.A. Overlap of swift heavy ion tracks in Al2O3. *Nuclear Instruments and Methods in Physics Research B.* 2018. Vol. 435, pp. 121–125.

20 Tao S., Chao H., Hailong D., et al. First principles study of structure, electronic and optical properties of Y3Fe5O12in cubic and trigonal phases. *Materials Science- Poland.* 2015. Vol. 33, pp. 169–174.

21 Henke B.L., Gullikson E.M., Davis J.C. X-Ray Interactions: Photoabsorption, Scattering, Transmission, and Reflection at E = 50-30,000 eV, Z = 1-92. *Atomic Data and Nuclear Data Tables.* 1993. Vol. 54, pp. 181–342.

22 Mott N.F., Massey H.S.W. *The Theory of Atomic Collisions*. London: Oxford University Press, 1985, 858 p.

23 Jenkins T. M. *Monte Carlo Transport of Electrons and Photons*. Boston, MA: Springer US, 1988, 656 p.

24 Wemple S.H., Blank S.L., Seman J.A., Biolsi W.A. Optical properties of epitaxial iron garnet thin films. *Physical Review B.* 1974. Vol. 9, pp. 2134–2144.

25 Littmark J.F., Ziegler J.P., Biersack U. *The Stopping and Range of Ions in Solids*. New York: Pergamon Press, 1985, 321 p.

26 Akkerman A., Boutboul T., Breskin A., et al. Inelastic Electron Interactions in the Energy Range 50 eV to 10 keV in Insulators: Alkali Halides and Metal Oxides. *physica status solidi (b).* 1996. Vol. 198, pp. 769–784.

27 Lide D.R. *CRC Handbook of chemistry and physics*, 84th ed. Boca Raton: CRC Press, 2003, 2616 p.

28 Medvedev N., Volkov A.E. Reconciling anomalously fast heating rate in ion tracks with low electron-phonon coupling. 2021. Available at: https://arxiv.org/abs/2109.04401v1.

Article accepted for publication 23.02.2022